A Real-Time Expectation Maximization Algorithm for Acquiring Multi-Planar Maps of Indoor Environments with Mobile Robots

Sebastian Thrun, Christian Martin, Yufeng Liu, Dirk Hähnel,
Rosemary Emery-Montemerlo, Deepayan Chakrabarti, Wolfram Burgard

***Abstract*— This paper presents a real-time algorithm for acquiring compact 3D maps of indoor environments, using a mobile robot equipped with range and imaging sensors. Building on previous work on real-time pose estimation during mapping [1], our approach extends the popular expectation maximization algorithm [2] to multi-surface models, and makes it amenable to real-time execution. Maps acquired by our algorithm consist of compact sets of textured polygons that can be visualized interactively. Experimental results obtained in corridor-type environments illustrate that compact and accurate maps can be acquired in real-time and in a fully automated fashion.**

***Index Terms*— Robotic mapping, mobile robots, perception, statistical techniques**

I. Introduction

THIS paper presents a real-time algorithm for generating three-dimensional maps of indoor environments, from range and camera measurements acquired by a mobile robot. A large number of indoor mobile robots rely on environment maps for navigation [3]. Most all existing algorithms for acquiring such maps operate in 2D. 2D maps may appear sufficient for navigation, given that most indoor mobile robots are confined to two-dimensional planes. However, modeling an environment in 3D has two important advantages: first, 3D maps facilitate the disambiguation of different places, since 3D models are richer than 2D models; second, 3D maps are better suited for users interested in the interior of a building, such as architects or human rescue workers that would like to familiarize themselves with an environment before entering it. For these and other reasons, modeling buildings in 3D has been a long-standing goal of researchers in computer vision [4], [5], [6], [7]. Generating such maps with robots would make it possible to acquire maps of environments inaccessible to people [8], [9], such as abandoned mines that have recently been mapped in 3D by mobile robots [10].

In robotic mapping, moving from 2D to 3D is not just a trivial extension. The most popular paradigm in 2D mapping to date are occupancy maps [11], [12], which represent environments by fine-grained grids. While this is feasible in 2D, in 3D the complexity of these representations pose serious scaling limitations [12]. Other popular representations in 2D involve point clouds [13], [14] or line segments [15]. Line representations have been generalized to 3D by representing maps through sets of fine-grained polygons [1], [9]. The resulting maps are often quite complex, and off-the-shelf computer graphics algorithms for mesh simplification [16] tend to generate maps that are visually inaccurate [1].

This paper presents an algorithm for recovering low-complexity 3D models from range and camera data that specifically exploits prior knowledge on the shape of basic building elements. In particular, our approach fits a probabilistic model that consists of large rectangular, flat surfaces to the data collected by a robot. Areas in the map that are not explained well by flat surfaces are modeled by small polygons (as in [9]), enabling our approach to accommodate non-flat areas in the environment. The resulting maps are less complex than those generated by the previous approaches discussed above. Moreover, by moving to a low-complexity model, the noise in the resulting maps is reduced—which is a side-effect of the variance reduction by fitting low-complexity models.

To identify low-complexity models, the approach presented here uses a real-time variant of the *expectation maximization* (EM) algorithm [2], [17]. Our algorithm simultaneously estimates the number of surfaces and their locations. Measurements not explained by any surface are mapped onto fine-grained polygonal representations, enabling our approach to model non-planar artifacts in the environment. The resulting map is represented in VRML format (virtual reality markup language), with texture superimposed from a panoramic camera.

Our approach rests on two key assumptions. First, it assumes that a good estimate of the robot pose is available. The issue of pose estimation (localization) in mapping has been studied extensively in the robotics literature [18]. In all our experiments, we use a real-time algorithm described in [1] to estimate pose; thus, our assumption is not unrealistic at all, but it lets us focus on the 3D mapping aspects of our work. Second, we assume that the environment is largely composed of flat surfaces. The flat surface assumption leads to a convenient close-form solution of the essential steps of our EM algorithm. Flat surfaces are commonly found in indoor environments, specifically in corridors. We also notice that our algorithm retains measurements that cannot be mapped onto any flat surface and maps them into finer grained polygonal approximations. Hence, the final map may contain non-flat regions in areas that are not sufficiently flat in the physical world.

Our approach has been fully implemented using the mobile robot shown in Figure 1a. This robot is equipped with

S. Thrun is with Stanford University, Y. Liu, R. Emery-Montemerlo, and D. Chakrabarti are with Carnegie Mellon University, C. Martin is with the University of Ilmenau, and W. Burgard and D. Hähnel are with the University of Freiburg.

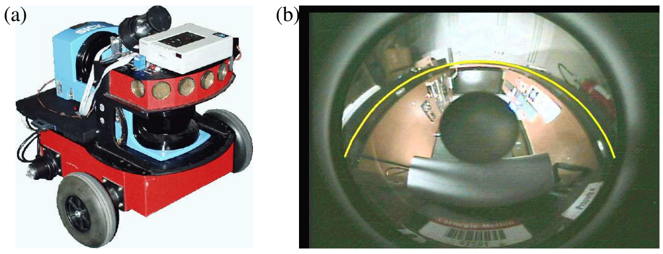

Fig. 1. Mobile robot, equipped with two 2D laser range finders and a panoramic camera. The camera uses a panoramic mirror mounted only a few centimeters away from the optical axis of the laser range finder.

a forward-pointed laser range finder for localization during mapping, an upward-pointed laser range finder for structural mapping, and a panoramic camera for recording the texture of the environment (see Figure 1b). The system has been tested in several different buildings. Our results illustrate that the algorithm is effective in generating compact and accurate 3D maps in real-time.

II. Generative Probabilistic Model

A. World Model

In our approach, 3D maps are composed of rectangular flat surfaces, representing doors, walls, ceilings, plus sets of small polygons representing non-flat surfaces. We will denote the set of rectangular flat surfaces by θ, where

$$\theta = \{\theta_1, \ldots, \theta_J\} \tag{1}$$

Here J is the total number of rectangular surfaces θ_j. Each θ_j is described by a total of nine parameters, arranged in three groups:

$$\theta_j = \langle \alpha_j, \beta_j, \gamma_j \rangle \tag{2}$$

The vector α_j is the three-dimensional surface normal of the surface; the value β_j is the one-dimensional offset between the surface and the origin of the coordinate system; and γ_j are five parameters specifying the size and orientation of the rectangular area within the (infinite) planar surface represented by α_j and β_j.

B. Measurements

Measurements are obtained using a laser range finder. Each range measurement is projected into 3D space, exploiting the fact that the robot pose is known. The 3D coordinate of the i-th range measurement will be denoted

$$z_i \in \Re^3 \tag{3}$$

We denote the set of all measurements by

$$Z = \{z_i\} \tag{4}$$

The Euclidean distance of any coordinate z_i in 3D space to any surface θ_j will be denoted

$$d(z_i, \theta_j) \tag{5}$$

In our implementation, we distinguish two cases: The case where the orthogonal projection of z_i falls into the rectangle, and the case where it does not. In the former case, $d(z_i, \theta_j)$ is given by $\alpha_j \cdot z_i - \beta_j$; in the latter case, $d(z_i, \theta_j)$ is the Euclidean distance between the bounding box of the rectangle and z_i, which is either a point-to-line distance or a point-to-point distance.

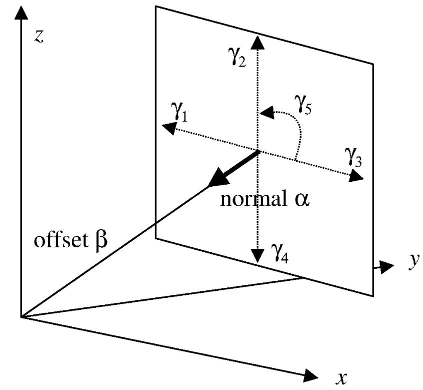

Fig. 2. Illustration of the parameters in the planar surface model, shown here for one surface.

C. Correspondences

In devising an efficient algorithm for environment mapping, it will prove convenient to make explicit the relation between individual measurements z_i and the different components θ_j of the model. This is achieved through *correspondence variables*. For each measurements C_i, we define there to be $J+1$ binary correspondence variables, collectively referred to as C_i.

$$C_i = \{c_{i*}, c_{i1}, c_{i2}, \ldots, c_{iJ}\} \tag{6}$$

The vector C_i specifies which part of the model θ "causes" the measurement z_i. Each of the variables in C_i is binary. The variable c_{ij} (for $1 \leq j \leq J$) is 1 if and only if the i-th measurement z_i corresponds to the j-th surface in the map, θ_j. If the measurement does not correspond to any of the surfaces in the map, the "special" correspondence variable c_{i*} is 1. This might be the case because of random measurement noise, or due to the presence of non-planar objects in the world.

Naturally, each measurement is caused by exactly one of those $J+1$ possible causes. This implies that the correspondences in C_i sum to 1:

$$c_{i*} + \sum_{j=1}^{J} c_{ij} = 1 \tag{7}$$

Our algorithm below involves a step in which probabilities over correspondences are calculated from the data.

D. Measurement Model

The *measurement model* ties together the volumetric map and the measurements Z. The measurement model is a probabilistic generative model of the measurements given the world:

$$p(z_i | C_i, \theta) \tag{8}$$

where C_i is the correspondence vector of the i-th measurement, and θ is the set of planar surfaces. Our approach assumes Gaussian measurement noise. Suppose $c_{ij} = 1$, that is, the measurement z_i corresponds to the surface θ_j in the model.

The error distribution is then given by the following normal distribution with variance parameter σ

$$p(z_i|c_{ij}=1,\theta) \quad := \quad \frac{1}{\sqrt{2\pi\sigma^2}}\, e^{-\frac{1}{2}\frac{d^2(z_i,\theta_j)}{\sigma^2}} \tag{9}$$

Notice that the log likelihood of this normal distribution is proportional to the squared Euclidean distance $d(z_i, \theta_j)$ between the measurement z_i and the surface θ_j.

The normal distributed noise is a good model if a range finder succeeds in detecting a flat surface. Sometimes, however, the object detected by a range finder does not correspond to a flat surface, that is, $c_{i*} = 1$. In our approach, we model such events using a uniform distribution over the entire measurement range:

$$p(z_i|c_{i*}=1,\theta) \quad := \quad \begin{cases} 1/z_{\max} & \text{if } 0 \le z_i \le z_{\max} \\ 0 & \text{otherwise} \end{cases} \tag{10}$$

The interval $[0; z_{\max}]$ denotes the measurement range of the range finder. The uniform noise model is clearly just a crude approximation, as real measurement noise is not uniform. However, uniform distributions are mathematically convenient and provide excellent results.

For reasons that shall become apparent below, we note that the uniform density in Equation (10) can be rewritten as follows:

$$\frac{1}{z_{\max}} \quad = \quad \frac{1}{\sqrt{2\pi\sigma^2}}\, e^{-\frac{1}{2}\log\frac{z_{\max}^2}{2\pi\sigma^2}} \tag{11}$$

Clearly, a uniform noise model is somewhat simplistic; however, it is mathematically convenient and was found to work well in our experiments.

III. The Log-Likelihood Function

To devise a likelihood function suitable for optimization, it shall prove useful to express the sensor model as the following exponential mixture:

$$p(z_i|C_i,\theta) = \frac{1}{\sqrt{2\pi\sigma^2}}\; e^{-\frac{1}{2}\left[c_{i*}\log\frac{z_{\max}^2}{2\pi\sigma^2}+\sum_j c_{ij}\frac{d^2(z_i,\theta_j)}{\sigma^2}\right]} \tag{12}$$

This form follows directly from Equations (9) and (11) and the assumption that exactly one variable in C_i is 1, whereas all others are zero. This form of the measurement model enables us to devise a compact expression of the *joint probability* of a measurement z_i along with its correspondence variables C_i:

$$p(z_i,C_i|\theta) = \frac{1}{(J+1)\sqrt{2\pi\sigma^2}} e^{-\frac{1}{2}\left[c_{i*}\log\frac{z_{\max}^2}{2\pi\sigma^2}+\sum_j c_{ij}\frac{d^2(z_i,\theta_j)}{\sigma^2}\right]} \tag{13}$$

Assuming independence in measurement noise, the likelihood of *all* measurements Z and their correspondences $C := \{C_i\}$ is then given by

$$p(Z,C|\theta) \tag{14}$$
$$= \prod_i \frac{1}{(J+1)\sqrt{2\pi\sigma^2}} e^{-\frac{1}{2}\left[c_{i*}\log\frac{z_{\max}^2}{2\pi\sigma^2}+\sum_j c_{ij}\frac{d^2(z_i,\theta_j)}{\sigma^2}\right]}$$

This equation is simply the product of (13) over all measurements z_i.

In EM, it is common practice to maximize the log-likelihood instead of the likelihood (14), exploiting the fact that the logarithm is monotonic in its argument:

$$\log p(Z,C|\theta) \;= \tag{15}$$
$$\sum_i \left[\log\frac{1}{(J+1)\sqrt{2\pi\sigma^2}} - \frac{1}{2}c_{i*}\log\frac{z_{\max}^2}{2\pi\sigma^2} - \frac{1}{2}\sum_j c_{ij}\frac{d^2(z_i,\theta_j)}{\sigma^2}\right]$$

Finally, while the formulas above all compute a joint over map parameters *and* correspondence, all we are actually interested in are the map parameters. The correspondences are only interesting to the extent that they determine the most likely map θ. Therefore, the goal of estimation is to maximize the *expectation* of the log likelihood (15), where the expectation is taken over all correspondences C. This value, denoted $E_C[\log p(Z,C|\theta)]$, is the expected log likelihood of the data given the map with the correspondences integrated out. It is obtained directly from Equation (15):

$$\begin{aligned} & E_C[\log p(Z,C|\theta) \mid Z,\theta] \\ & \quad = \sum_i \left[\log\frac{1}{(J+1)\sqrt{2\pi\sigma^2}} - \frac{1}{2}E[c_{i*}|z_i,\theta]\log\frac{z_{\max}^2}{2\pi\sigma^2} \right. \\ & \qquad \left. - \frac{1}{2}\sum_j E[c_{ij}|z_i,\theta]\frac{d^2(z_i,\theta_j)}{\sigma^2}\right] \end{aligned} \tag{16}$$

In [19], it is shown that maximizing this expectation indeed maximizes the log likelihood of the data.

IV. Likelihood Maximization Via EM

The expected log-likelihood (16) is maximized using EM, a popular method for hill climbing in likelihood space for problems with latent variables [2]. EM generates a sequence of maps, $\theta^{[0]}, \theta^{[1]}, \theta^{[2]}, \ldots$. Each map improves the log-likelihood of the data over the previous map until convergence. More specifically, EM starts with a random map $\theta^{[0]}$. Each new map is obtained by executing two steps: an E-step, where the expectations of the unknown correspondences $E[c_{ij}|\theta^{[n]}, z_i]$ and $E[c_{i*}|\theta^{[n]}, z_i]$ are calculated for the n-th map $\theta^{[n]}$, and an M-step, where a new maximum likelihood map $\theta^{[n+1]}$ is computed under these expectations.

A. The E-Step

In the E-step, we are given a map $\theta^{[n]}$ for which we seek to determine the expectations $E[c_{ij}|\theta^{[n]}, z_i]$ and $E[c_{i*}|\theta^{[n]}, z_i]$ for all i, j. Bayes rule, applied to the sensor model, gives us a way to calculate the desired expectations (assuming a uniform prior over correspondences for mathematical convenience):

$$\begin{aligned} e_{ij}^{[n]} \quad &:= \quad E[c_{ij}|\theta^{[n]}, z_i] \;=\; p(c_{ij}|\theta^{[n]}, z_i) \\ &= \quad \frac{p(z_i|\theta^{[n]}, c_{ij})\,p(c_{ij}|\theta^{[n]})}{p(z_i|\theta^{[n]})} \\ &= \quad \frac{e^{-\frac{1}{2}\frac{d^2(z_i,\theta_j)}{\sigma^2}}}{e^{-\frac{1}{2}\log\frac{z_{\max}^2}{2\pi\sigma^2}} + \sum_k e^{-\frac{1}{2}\frac{d^2(z_i,\theta_k)}{\sigma^2}}} \end{aligned} \tag{17}$$

and similarly

$$e_{i*}^{[n]} := E[c_{i*}|\theta^{[n]}, z_i] = \frac{e^{-\frac{1}{2}\log\frac{z_{\max}^2}{2\pi\sigma^2}}}{e^{-\frac{1}{2}\log\frac{z_{\max}^2}{2\pi\sigma^2}} + \sum_k e^{-\frac{1}{2}\frac{d^2(z_i,\theta_k)}{\sigma^2}}} \quad (18)$$

As pointed out in [17], [19], substituting these expectations into the log-likelihood (16) lower-bounds the log-likelihood by a function tangent to it at $\theta^{[n]}$.

B. The M-Step

In the M-step, this lower bound is optimized. More specifically, we are given the expectations $e_{ij}^{[n]}$ and $e_{i*}^{[n]}$ and seek to calculate a map $\theta^{[n+1]}$ that maximizes the expected log-likelihood of the measurements, as given by Equation (16). In other words, we seek surface parameters $\langle\alpha^{[n+1]}, \beta^{[n+1]}, \gamma^{[n+1]}\rangle$ that maximize the expected log-likelihood of the map under fixed expectations $e_{ij}^{[n]}$ and $e_{i*}^{[n]}$.

Obviously, many of the terms in (16) do not depend on the map parameters θ. This allows us to simplify (16) and instead carry out the following minimization:

$$\theta^{[n+1]} = \underset{\theta}{\operatorname{argmin}} \sum_i \sum_j e_{ij}^{[n]} d^2(z_i, \theta_j) \quad (19)$$

The actual M-step proceeds in two steps. First, our approach determines the parameters $\alpha_j^{[n+1]}$ and $\beta_j^{[n+1]}$, which specify the principal orientation and location of the rectangular surface without the surface boundary. If walls are assumed to be boundless, the minimization (19) is equivalent to the minimization

$$\langle\alpha^{[n+1]}, \beta^{[n+1]}\rangle = \underset{\alpha,\beta}{\operatorname{argmin}} \sum_i \sum_j e_{ij}^{[n]} (\alpha_j \cdot z_i - \beta_j)^2 \quad (20)$$

subject to the normality constraints $\alpha_j \cdot \alpha_j = 1$, for all j. This quadratic optimization problem is commonly solved via Lagrange multipliers λ_j for $j = 1, \ldots, J$ [20], [21]:

$$L := \sum_i \sum_j e_{ij}^{[n]} (\alpha_j \cdot z_i - \beta_j)^2 + \sum_j \lambda_j \alpha_j \cdot \alpha_j \quad (21)$$

Obviously, for each minimum of L, it must be the case that $\frac{\partial L}{\partial \alpha_j} = 0$ and $\frac{\partial L}{\partial \beta_j} = 0$. Setting the derivatives of L to zero leads to the linear system of equalities:

$$\sum_i e_{ij}^{[n]} (\alpha_j^{[n+1]} \cdot z_i - \beta_j^{[n+1]}) z_i - \lambda_j \alpha_j^{[n+1]} = 0 \quad (22)$$

$$\sum_i e_{ij}^{[n]} (\alpha_j^{[n+1]} \cdot z_i - \beta_j^{[n+1]}) = 0 \quad (23)$$

$$\alpha_j^{[n+1]} \cdot \alpha_j^{[n+1]} = 1 \quad (24)$$

The values of $\beta_j^{[n+1]}$ is obtained from Equations (22) and (23):

$$\beta_j^{[n+1]} = \frac{\sum_k e_{kj}^{[n]} \alpha_j^{[n+1]} \cdot z_k}{\sum_k e_{kj}^{[n]}} \quad (25)$$

Substituting those back into (22) gives us

$$\sum_i e_{ij}^{[n]} \left(\alpha_j^{[n+1]} \cdot z_i - \frac{\sum_k e_{kj}^{[n]} \alpha_j^{[n+1]} \cdot z_k}{\sum_k e_{kj}^{[n]}} \right) z_i = \lambda_j \alpha_j^{[n+1]} \quad (26)$$

This is a set of linear equations of the type

$$A_j^{[n]} \cdot \alpha_j^{[n+1]} = \lambda_j \alpha_j^{[n+1]} \quad (27)$$

where each $A_j^{[n]}$ is a 3×3 matrix whose elements are as follows:

$$a_{st}^{[n]} = \sum_i e_{ij}^{[n]} z_{is} z_{it} - \frac{\sum_i e_{ij}^{[n]} z_{it} \sum_k e_{kj}^{[n]} z_{ks}}{\sum_k e_{kj}^{[n]}} \quad (28)$$

for $s, t \in \{1, 2, 3\}$, subject to (24). It is now easy to see that each solution of (27) must be an eigenvector of $A_j^{[n]}$. The two eigenvectors with the largest eigenvalues describe the principle orientation of the surface. The third eigenvector, which corresponds to the smallest eigenvalue, is the normal vector of this surface, hence our desired solution for $\alpha_j^{[n+1]}$.

Finally, the M-step calculates new bounding boxes $\gamma_j^{[n+1]}$. It does so by determining the minimum rectangular box on the surface which includes all points whose maximum likelihood assignment is the j-th surface θ_j:

$$\{z_i, \text{such that } j = \underset{k \in 1,\ldots,J,*}{\operatorname{argmax}} e_{i,k}^{[n]}\} \quad (29)$$

This optimization problem does not possess an easy closed-form solution. Our approach probes the orientation in 1-degree intervals, then calculates he tightest bounding box for each orientation. The bounding box with the smallest enclosed surface volume is finally selected. This step leads to a near-optimal rectangular surface that contains all measurements that most likely correspond to the surface at hand.

C. Determining the Number of Surfaces

Parallel to computing the surface parameters, our approach determines the number of surfaces J. Our approach is based on a straightforward Bayesian prior that penalizes complex maps using an exponential prior, written here in log-likelihood form:

$$p(\theta|Z) \propto p(Z|\theta) - \kappa J \quad (30)$$

Here κ is a constant factor. The final map estimator is, thus, a maximum posterior probability estimator (MAP), which combines the complexity-penalizing prior with the data likelihood calculated by EM. In practice, this approach implies that surfaces not supported by sufficiently many data measurements (weighted by their expectation) are discarded. This makes it possible to choose the number of rectangular surfaces J concurrently with the execution of the EM algorithm.

In our implementation, the search for the best J is interleaved with running the EM algorithm. The search involves a step for creating new surfaces, and another one for terminating surfaces, both executed in regular intervals (every 20 iterations in our offline implementation). In the surface creation step, new surfaces are created based on measurements z_i that are poorly explained by the existing model. A measurement z_i is considered poorly explained if its value e_{i*} exceeds a threshold, indicating that none of the planar surfaces in the model explain the measurement well. A new surface is started if three adjacent measurements are poorly explained; the initial parameters of this new surface are then uniquely determined through the coordinates of these three measurements. The

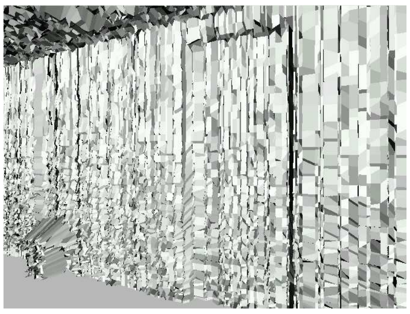

Fig. 3. Polygonal map generated from raw data, not using EM. The display without texture shows the level of noise involved. In particular, it illustrates the difficulty of separating the door from the nearby wall (as achieved by EM).

number of new surfaces is kept limited at each iteration, using random selection among all candidates if the number of candidate surfaces exceeds the total limit. The new surfaces are then added to the model and treated identically to all other surfaces in subsequent iterations of EM.

In the termination step, each surface undergoes a posterior evaluation using the criterion set forth in Equation (30). If removing a surface or fusing it with a nearby surface *increases* the posterior in Equation (30), the corresponding action is taken. Otherwise, it is retained in the model. In this way, only surfaces supported by sufficiently many data points survive the selection process, avoiding the overfitting that inevitably would occur without a complexity penalty term.

D. Texture Mapping and Visualization

Textures are extracted from the panoramic camera, along a stripe shown in Figure 1b that corresponds to the range measurement taken by the vertical laser range finder. These stripes are collected at frame rate and pasted together into raw texture maps. These maps are then mapped onto the planar surfaces in real-time, using a technique analogous to the one described in [22]. Textures of the same feature in the environment recorded at different points in time are presently not merged due to tight computational constraints—which is a clear shortcoming of our present implementation.

The final model contains all surfaces in θ; however, it lacks information on non-flat objects in the environment. The final 3D visualization of the environment is enriched by fine-grained polygonal models of such non-flat objects. In particular, our approach analyzes all measurements whose most likely correspondence is the class "$*$." For any occurrence of three nearby such measurements. a small triangle is introduced into the final 3D visualization. In this way, the visualization contains not only large flat surfaces, but also fine-grained polygonal models of non-flat objects in the environment. The final output of our program is a VRML file, which makes it possible to render the 3D model using off-the-shelf software.

V. Online EM

Our approach has been extended into an online algorithm that enables robots to acquire compact 3D models in real-time (see [23]). EM, as presented so far, is inherently offline. It required multiple passes through the data set. As the data set grows, so does the computation per iteration of EM. This limitation is a common limitation of the vanilla EM algorithm [19].

The key insight that leads to an online implementation is that during each fixed time interval, only a constant number of new range measurements arrive (collectively referred to as z_i). If we begin our estimation with the model acquired in the first $i-1$ measurements, only constantly many new measurement values have to be incorporated into the model in response to observing z_i. Such a routine would be strictly incremental; however, it would fail to adjust correspondence variables based on data acquired at a later point in time. Our approach is slightly more sophisticated in that it adjusts past expectations, but it does this in a way that still conforms to constant update time.

A. Online E-Step

The online E-step considers only a finite subset of all measurements, and only calculates expectations for the correspondence variables of those measurements. In particular, it includes all new range measurements, of which there are only finitely many. Additionally, it includes past measurements that meet the following condition: They lie at the boundary of two surfaces (judging from their maximum likelihood assignments) or they are entirely unexplained by any existing surface. These conditions alone are insufficient to assure constant time computation. Thus, we also attach a counter to each measurement that keeps track of the total number of times it was considered in an E-step calculation. If this counter exceeds a threshold, the expected correspondence value is frozen and never recalculated again. It is easy to see that the last condition ensures constant time update (in expectation). The former condition identifies "interesting" measurements, which greatly reduces the constant factor in the computational complexity.

B. Online M-Step

The online M-step is slightly more complex. This is because as the data set grows, so do two things: the number of model components J and the number of measurements z_i associated with each model component. Each of these expansions have to be controlled to ensure that the M-step can be executed in real-time.

In the online M-step, only a small number of "active" surfaces are re-estimated. We say that a surface θ_j is active at time i if the E-step executed at that time changed, for any of the updated measurements, the maximum likelihood correspondence to or away from the surface θ_j. Clearly, this is an approximation, in that any adjustment of the expected correspondence affects all model parameters, at least in principle. However, our approach is a good approximation that limits the number of surfaces considered in the M-step to a constant number.

Finally, our approach addresses the fact that the number of points involved in each maximization grows over time. In conventional EM, every measurement participates in the calculation of all surface parameters, though most make only a negligible contribution. To reduce the number of measurements used in the M-Step, our online approach considers only those whose maximum likelihood data association corresponds to the model component in question. This is analogous to the well-known k-means algorithm [24] for clustering, which approximates the EM algorithm using hard assignments. Furthermore, if the number of maximum likelihood measurements exceeds a threshold, our approach randomly subsamples those measurements. By doing so, the amount of computation when recalculating the parameters of a model component is bounded by a constant number, as is the overall computational complexity of the M-Step.

(a) Fine-grained polygonal maps generated from raw data

(b) Low-complexity maps generated using EM

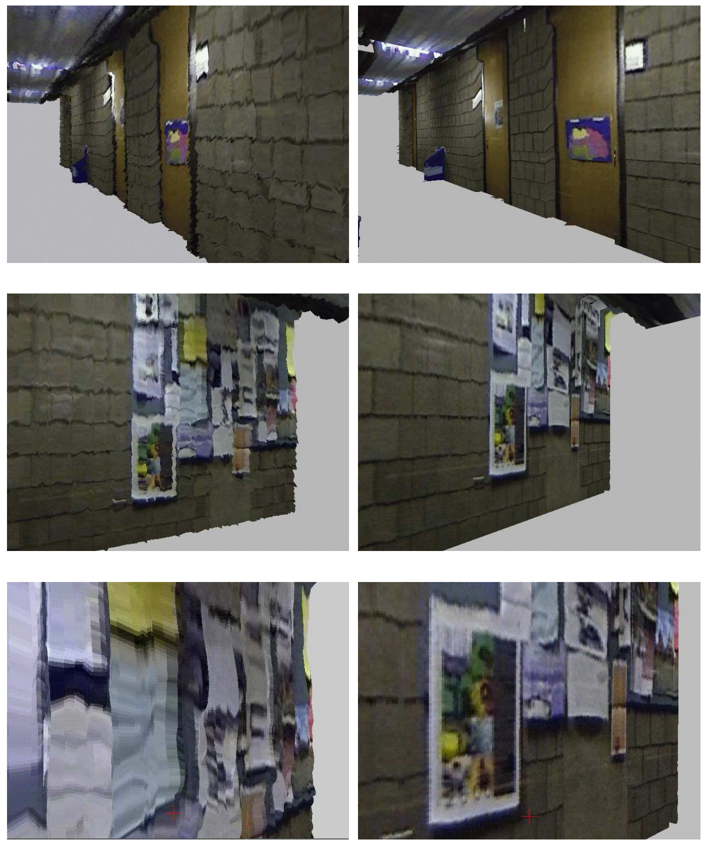

Fig. 4. 3D map generated (a) from raw sensor data, and (b) using the offline version of EM. In this map. 94.6% of all measurements are explained by 7 surfaces. Notice that the map in (b) is smoother and appears to be visually more accurate than the one in (a).

C. Online Model Selection

Finally, our approach also implements Bayesian model selection in real-time. New surfaces are introduced for new measurements which are not "explained" by any of the existing surfaces in the map. A measurement is explained by an existing surface if its likelihood of having been generated from that surface is above a threshold; otherwise it will be used to seed a new surface. Surfaces are removed from the map if after a fixed number of iterations they are not supported by sufficiently many measurements, in accordance with the map complexity penalty factor κ set forth in Equation (30). As a result, the number of surfaces J increases with the complexity of the environment, while all computation can still be carried out online, irrespective of the total map size.

The resulting algorithm is strictly incremental. It has been implemented on a low-end laptop PC, where it is able to construct compact 3D maps in real-time.

VI. Experimental Results

Our experiments were carried out in two stages: First, we implemented and evaluated the offline EM algorithm. This evaluation served us to establish the basic capability of extracting large planar surfaces from complex data sets using EM. Our second set of experiments was carried out in real-time using the online version of our approach.

All computation in these experiments was carried out onboard the moving robot platform shown in Figure 1. As noted above, the robot is equipped with two SICK PLS laser range finders, one pointed forward and one pointed upward, perpendicular to the robot's motion direction. The SICK sensor covers an area of 180 degrees with a one-degree angular resolution. The range accuracy is described by the manufacturer as ± 5 centimeters. The sampling rate in our experiments is approximately 5 Hertz (entire scans).

A. Offline EM

The offline version of EM was tested using a data set acquired inside a university building. The data set consists of 168,120 range measurements and 3,270 camera images, collected in less than two minutes. In a pre-alignment phase, our software extracted 3,220,950 pixels, all of which directly correspond to range measurements. Nearby scans were converged into polygons. Figure 3 shows a detail of the resulting map without the texture superimposed. This figure clearly illustrates the high level of noise in the raw data. The left column of Figure 4 shows three views of the map with texture superimposed.

The result of our EM algorithm is shown in the right column of Figure 4. This specific map contains of $J = 7$ flat surfaces, which together account for 94.6% of all measurements. Clearly, the new map is smoother and visually more accurate. It also models non-planar regions well, as manifested by a trash-bin in the top panel of that figure, which is not modeled by a planar surface. The corresponding measurements are not mapped to any of the surfaces θ_i. Figure 5 show the corresponding map segment, illustrating that importance of merging flat surfaces with fine-grained polygons for modeling building interiors. Notice also that the wall surface is different from the door surface. A small number of measurements in the door surface are erroneously assigned to the wall surface. The poster board shown in various panels of Figure 4 highlights once again the benefits of the EM approach over the raw data maps: Its visual accuracy is higher thanks to the planar model on which the texture is being projected.

Figure 6 shows the number of surfaces J and the number of measurements explained by these surfaces, as a function of the iteration. Every 20 steps (in expectation), surfaces are terminated and restarted. After only 500 iterations, the number of surfaces settles around a mean (and variance) of 8.76 ± 1.46, which explains a steady $95.5 \pm 0.006\%$ of all measurements.

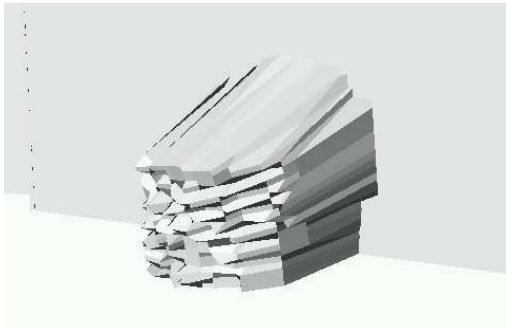

Fig. 5. Model of a trash bin in the final map, with a large planar rectangular surface patch in the background. Our algorithm recognizes that this object cannot be explained by planar surfaces with sufficient likelihood, hence it retains the fine-grained polygonal representation.

2,000 iterations require approximately 20 minutes computation on a low-end PC.

B. Real-Time Implementation

The real-time implementation using online EM was evaluated more thoroughly and in several different buildings. Overall, we found our approach to be highly reliable in generating accurate maps. Figure 7 illustrates the online creation of compact maps. Shown in the left column are maps generated directly from the raw measurement data by creating polygons for any set of nearby measurements. The right column shows a sequence of maps built in real-time, using our incremental EM algorithm. We note that this specific illustration shows only vertical surfaces; however, our implementation handles surfaces in arbitrary orientations.

As it is easily seen, the new map is more compact than the raw data map. A small number of surfaces suffices to model the vast amounts of data. Close inspection of Figure 7 illustrates EM at work. For example, a small region in Figure 7i has not been identified as belonging to a flat wall, simply because the amount of noise in the rectangular surface below this patch is too large. Further optimization of this past data leads to a more compact map, as illustrated in Figure 7j.

Figure 8 shows views of a compact 3D map acquired in real-time, for the same environment as reported previously. The entire data collection requires less than 2 minutes, during which all processing occurs.

As is easily seen, the identification of rectangular surfaces in the environment has a positive effect of the visual acuity of the map. Figure 9 shows inside projections of a 3D map built by EM and compares it to a map built without EM, using fine-grained polygonal maps, and using data sets obtained in two different university buildings. Obviously, the visual accuracy of the texture projected onto flat surfaces is higher than the renderings obtained from the fine-grained polygonal map. This illustrates once again that the resulting map is not only more compact but it also provides more visual detail than the map created without our approach.

In an attempt to quantitatively evaluate our approach, we mapped three different corridor environments in different buildings. The complexity of those environments was comparable to the maps shown here. The number of initial polygons was between $3.5{\cdot}10^4$ and $6.5{\cdot}10^4$. The final maps contained on average 0.60% as many polygons (0.69%, 0.80%, and 0.32%), which corresponds to an average compression ratio of $1:192$. Overall, we found that the online version generated an order of magnitude more flat surfaces J than the offline version. This increased number was partially due to a lower penalty term κ. An additional cause of the increase in J was the fact that the online version considers splitting and fusion decisions only for a brief time period. Overall, the increased number of surfaces J led to a decrease in the overall complexity of the map, thanks to the fact that significantly more measurements were explained by surfaces θ_j found by EM.

(a) Map complexity (number of surfaces J)

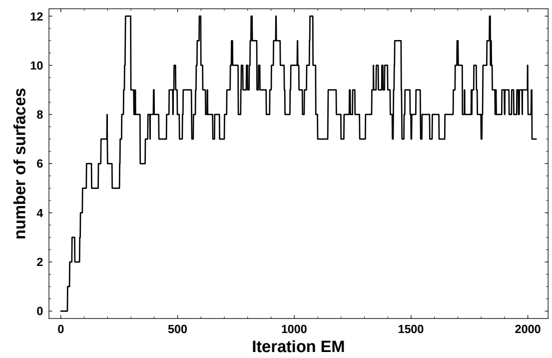

(b) Percentage of measurements explained by those surfaces

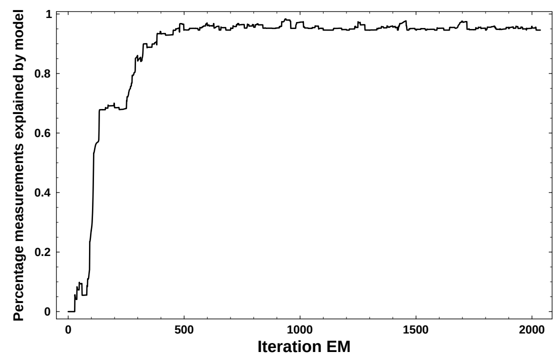

Fig. 6. Offline EM: (a) number of surfaces J and (b) percentage of points explained by those surfaces as function of the iterator. A good map is available after 500 iterations.

We finally note that all computation in our experiment was carried out on a single laptop on board the robot. The views in Figures 7 through 9 were rendered using a standard software package for rendering VRML models.

VII. Related Work

As argued in the introduction to this article, the vast majority of robot modeling research has focused on building maps in 2D. Our approach is reminiscent of an early paper by Chatila and Laumond [15] and a related paper by Crowley [25], who proposed to reconstruct low-dimensional line models in 2D from sensor measurements. Our work is also related to work on line extraction from laser range scans [26]. However, these methods address the two-dimensional case, where lines can be extracted from a single scan.

(a) Raw data map (15 scans)

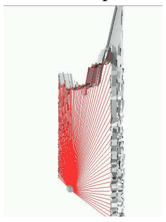

(f) Map with online EM (15 scans)

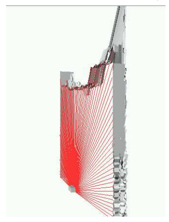

(b) Raw data map (43 scans)

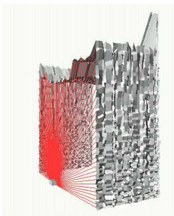

(g) Map with online EM (43 scans)

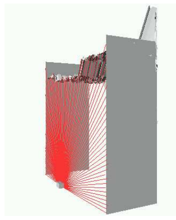

(c) Raw data map 62 scans)

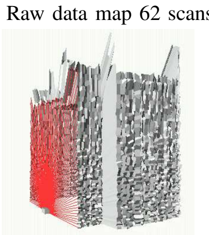

(h) Map with online EM (62 scans)

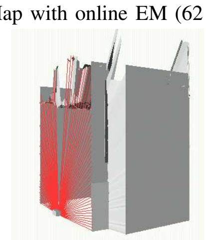

(d) Raw data map (172 scans)

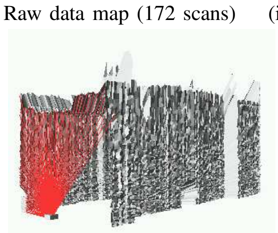

(i) Map with online EM (172 scans)

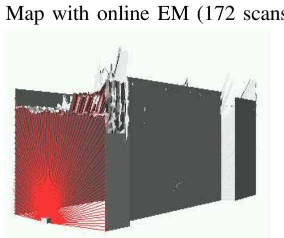

(e) Raw data map (274 scans)

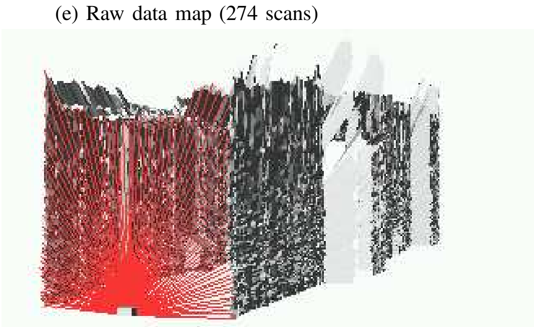

(j) Map with online EM (274 scans)

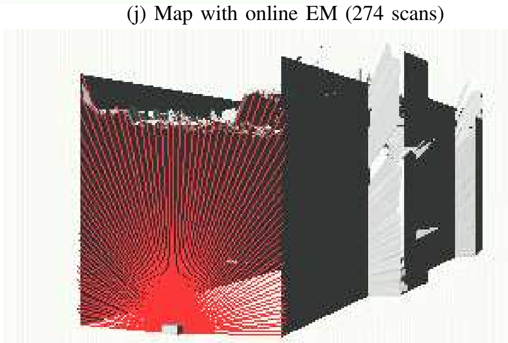

Fig. 7. Raw data (left column) and maps generated using online EM (right column). The red lines visualize the most recent range scan. Some of the intermediate maps exhibit suboptimal structures, which are resolved in later iterations of EM. Despite this backwards-correction of past estimates, the algorithm presented in this paper still runs in real-time, due to careful selection of measurements that are considered in the EM estimation.

Fig. 8. Views of a compact 3D texture map built in real time with an autonomously exploring robot.

In the area of computer vision, object recognition under geometric constraints (such as the planar surface assumption) is a well-researched field [27], [28], [29]. Multiple researchers have studied the topic of 3D scene reconstruction from data. Approaches for 3D modeling can roughly be divided into two categories: Methods that assume knowledge of the pose of the sensors [4], [5], [6], [30], [31], and methods that do not [32]. Of great relevance is a paper by Roth and Wibowo [33], who have also proposed the use of a mobile platform to acquire textured 3D models of the environment. Their systems includes a 3D range sensor and eight cameras. Just like our system, theirs uses sensor information to compensate odometric errors. Their approach, however, does not consider the uncertainty of individual measurements when generating the 3D model.

Our approach is somewhat related to [34], which reconstructs planar models of indoor environments using stereo vision, using some manual guidance in the reconstruction process to account for the lack of visible structure in typical indoor environments. Like ours, the environment model is composed of flat surfaces; however, due to the use of stereo vision, the range data is too incomplete to allow for a fully automated modeling process to take place. Consequently, the technique in [34] relies on manual guidance in the process of identifying planar surfaces. Related work on outdoor terrain modeling can be found in [7], [35].

(a) Raw data map (using a high-accuracy range finder)

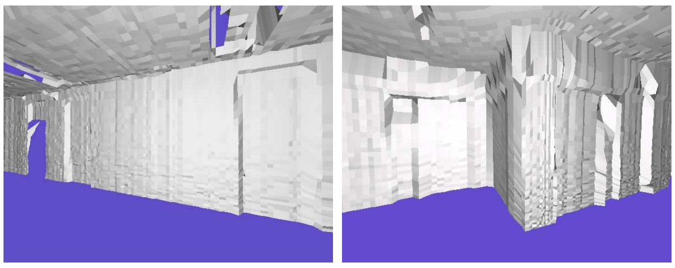

(b) Planes, extracted from the map using EM

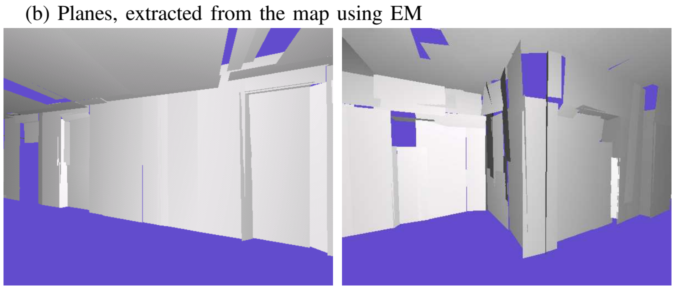

(c) Plane boundaries

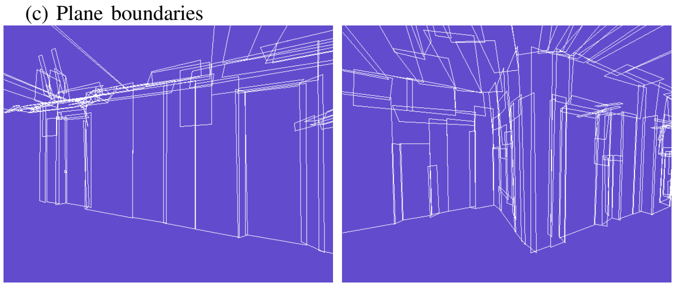

(d) Full texture map (planes only)

Fig. 9. Maps generated in real-time, of office environments at Carnegie Mellon University's Wean Hall (left column) and Stanford University's Gates Hall (right column).

VIII. Conclusion

We have presented an online algorithm for building compact maps of building interiors. This approach utilizes the expectation maximization algorithm for finding rectangular surface patches in 3D data, acquired by a moving robot equipped with laser range finders and a panoramic camera. While EM is traditionally an offline algorithm, a modified version of EM was presented, which is capable of generating such maps online, while the robot is in motion. This approach retains the key advantage of EM—namely the ability to revise past assignments and map components based on future data—while simultaneously restricting the computation in ways that make it possible to run the algorithm in real-time, regardless of the size of the map. Experimental results illustrate that this approach enables mobile robots to acquire compact and accurate maps of corridor-style indoor environments in real-time.

All results shown in this article were obtained using accurate 2D laser range finders. The mathematical approach can accommodate a wider array of range finders, such as sonars and range cameras, assuming that the sensor model is adjusted appropriately. However, we suspect that the high spatial and angular resolution of our laser ranges finder plays an important role in the success of our approach.

Although stated here in the context of finding rectangular flat surfaces, the EM algorithm is more general in that it can easily handle a richer variety of geometric shapes. The extension of our approach to richer classes of objects is subject to future research. Another topic of future research is to augment the EM algorithm to estimate the robot's location during mapping, as described in [36].

Finally, it would be worthwhile to include both laser's data in the mapping process. Unfortunately, the upward-pointed laser may never observe the same aspect of the environment twice; hence, further assumptions (such as smoothness) would be necessary to utilize its data. It would also be interesting to add the robot pose variables as latent variables in the EM algorithm, so that localization and modeling can be interleaved, as in see [36]. Unfortunately, the added computational complexity incurred by such extensions would make it difficult to execute the resulting algorithm online and in real-time.

Acknowledgment

This research is sponsored by by DARPA's MARS Program (Contracts N66001-01-C-6018 and NBCH1020014) and the National Science Foundation (CAREER grant IIS-9876136 and regular grant IIS-9877033), all of which is gratefully acknowledged. We also thankg three anonymous reviewers for insightful comments on an earlier version of this manuscript.

References

[1] S. Thrun, "A probabilistic online mapping algorithm for teams of mobile robots," *International Journal of Robotics Research*, vol. 20, no. 5, pp. 335–363, 2001.

[2] A. Dempster, A. Laird, and D. Rubin, "Maximum likelihood from incomplete data via the EM algorithm," *Journal of the Royal Statistical Society, Series B*, vol. 39, no. 1, pp. 1–38, 1977.

[3] D. Kortenkamp, R. Bonasso, and R. Murphy, Eds., *AI-based Mobile Robots: Case studies of successful robot systems*. Cambridge, MA: MIT Press, 1998.

[4] R. Bajcsy, G. Kamberova, and L. Nocera, "3D reconstruction of environments for virtual reconstruction," in *Proc. of the 4th IEEE Workshop on Applications of Computer Vision*, 2000.

[5] P. Debevec, C. Taylor, and J. Malik, "Modeling and rendering architecture from photographs," in *Proc. of the 23rd International Conference on Computer Graphics and Interactive Techniques (SIGGRAPH)*, 1996.

[6] H. Shum, M. Han, and R. Szeliski, "Interactive construction of 3D models from panoramic mosaics," in *Proc. of the International Conference on Computer Vision and Pattern Recognition (CVPR)*, 1998.

[7] S. Teller, M. Antone, Z. Bodnar, M. Bosse, S. Coorg, M. Jethwa, and N. Master, "Calibrated, registered images of an extended urban area," in *Proceedings of the Conference on Computer Vision and Pattern Recognition (CVPR)*, 2001.

[8] J. Casper, "Human-robot interactions during the robot-assisted urban search and rescue response at the world trade center," Master's thesis, Computer Science and Engineering, University of South Florida, Tampa, FL, 2002.

[9] M. Montemerlo, H. D, D. Ferguson, R. Triebel, W. Burgard, S. Thayer, W. Whittaker, and S. Thrun, "A system for three-dimensional robotic mapping of underground mines," Carnegie Mellon University, Computer Science Department, Pittsburgh, PA, Tech. Rep. CMU-CS-02-185, 2002.

[10] S. Thrun, D. Hähnel, D. Ferguson, M. Montemerlo, R. Triebel, W. Burgard, C. Baker, Z. Omohundro, S. Thayer, and W. Whittaker, "A system for volumetric robotic mapping of abandoned mines," in *Proceedings of the IEEE International Conference on Robotics and Automation (ICRA)*, 2003.

[11] A. Elfes, "Occupancy grids: A probabilistic framework for robot perception and navigation," Ph.D. dissertation, Department of Electrical and Computer Engineering, Carnegie Mellon University, 1989.

[12] H. P. Moravec, "Sensor fusion in certainty grids for mobile robots," *AI Magazine*, vol. 9, no. 2, pp. 61–74, 1988.

[13] J.-S. Gutmann and K. Konolige, "Incremental mapping of large cyclic environments," in *Proceedings of the IEEE International Symposium on Computational Intelligence in Robotics and Automation (CIRA)*, 2000.

[14] F. Lu and E. Milios, "Globally consistent range scan alignment for environment mapping," *Autonomous Robots*, vol. 4, pp. 333–349, 1997.

[15] R. Chatila and J.-P. Laumond, "Position referencing and consistent world modeling for mobile robots," in *Proceedings of the 1985 IEEE International Conference on Robotics and Automation*, 1985.

[16] M. Garland and P. Heckbert, "Simplifying surfaces with color and texture using quadric error metrics," in *Proceedings IEEE Visualization*, 1998.

[17] G. McLachlan and T. Krishnan, *The EM Algorithm and Extensions*. New York: Wiley Series in Probability and Statistics, 1997.

[18] J. Leonard, J. Tardós, S. Thrun, and H. Choset, Eds., *Workshop Notes of the ICRA Workshop on Concurrent Mapping and Localization for Autonomous Mobile Robots (W4)*. Washington, DC: ICRA Conference, 2002.

[19] R. Neal and G. Hinton, "A view of the EM algorithm that justifies incremental, sparse, and other variants," in *Learning in Graphical Models*, M. Jordan, Ed. Kluwer Academic Press, 1998.

[20] D. Eberly, *3D Game Engine Design: A Practical Approach to Real-Time Computer Graphics*. Morgan Kaufman/Academic Press, 2001.

[21] Y. Liu, R. Emery, D. Chakrabarti, W. Burgard, and S. Thrun, "Using EM to learn 3D models with mobile robots," in *Proceedings of the International Conference on Machine Learning (ICML)*, 2001.

[22] S. Nayar, "Omnidirectional vision," in *Proceedings of the Ninth International Symposium on Robotics Research*, Shonan, Japan, 1997.

[23] C. Martin and S. Thrun, "Online acquisition of compact volumetric maps with mobile robots," in *IEEE International Conference on Robotics and Automation (ICRA)*. Washington, DC: ICRA, 2002.

[24] R. Duda and P. Hart, *Pattern classification and scene analysis*. New York: Wiley, 1973.

[25] J. Crowley, "World modeling and position estimation for a mobile robot using ultrasonic ranging," in *Proceedings of the 1989 IEEE International Conference on Robotics and Automation*, Scottsdale, AZ, May 1989, pp. 674–680.

[26] F. Lu and E. Milios, "Robot pose estimation in unknown environments by matching 2d range scans," *Journal of Intelligent and Robotic Systems*, vol. 18, pp. 249–275, 1998.

[27] W. Grimson, *Object Recognition by Computer: The Role of Geometric Constraints*. Boston, MA: MIT Press, 1991.

[28] O. Faugeras, *Three-Dimensional Computer Vision, A Geometric Viewpoint*. Boston, MA: MIT Press, 1993.

[29] A. R. Pope, "Model-based object recognition - A survey of recent research," University of British Columbia, Department of Computer Science, Vancouver, Canada, Tech. Rep. TR-94-04, 1994.

[30] P. Allen and I. Stamos, "Integration of range and image sensing for photorealistic 3D modeling," in *Proceedings of the IEEE International Conference on Robotics and Automation (ICRA)*, 2000, pp. 1435–1440.

[31] S. Becker and M. Bove, "Semiautomatic 3-D model extraction from uncalibrated 2-D camera views," in *Proc. of the SPIE Symposium on Electronic Imaging, San Jose*, 1995.

[32] S. El-Hakim, P. Boulanger, F. Blais, and J.-A. Beraldin, "Sensor based creation of indoor virtual environment models," in *Proc. of the 4th Internetional Conference on Virtual Systems and Multimedia (VSMM)*, Geneva, Switzerland, 1997.

[33] G. Roth and R. Wibowo, "A fast algorithm for making mesh-models from multiple-view range data," in *Proceedings of the DND/CSA Robotics and Knowledge Based Systems Workshop*, 1995.

[34] L. Iocchi, K. Konolige, and M. Bajracharya, "Visually realistic mapping of a planar environment with stereo," in *Proceesings of the 2000 International Symposium on Experimental Robotics*, Waikiki, Hawaii, 2000.

[35] Y.-Q. Cheng, E. Riseman, X. Wang, R. Collins, and A. Hanson, "Three-dimensional reconstruction of points and lines with unknown correspondence across images," *International Journal of Computer Vision*, 2000.

[36] S. Thrun, D. Fox, and W. Burgard, "A probabilistic approach to concurrent mapping and localization for mobile robots," *Machine Learning*, vol. 31, pp. 29–53, 1998, also appeared in Autonomous Robots 5, 253–271 (joint issue).